

Spatially Heterogeneous Dynamics and the Adam–Gibbs Relation in the Dzugutov Liquid

Yeshitla Gebremichael,^{†,§} Michael Vogel,^{†,⊥} Magnus N. J. Bergroth,[†] Francis W. Starr,^{‡,||} and Sharon C. Glotzer^{*,†}*Departments of Chemical Engineering and Materials Science and Engineering, University of Michigan, Ann Arbor, Michigan 48109 and Department of Physics, Wesleyan University, Middletown, Connecticut 06459**Received: July 8, 2004; In Final Form: May 23, 2005*

We perform molecular dynamics simulations of a one-component glass-forming liquid and use the inherent structure formalism to test the predictions of the Adam–Gibbs (AG) theory and to explore the possible connection between these predictions and spatially heterogeneous dynamics. We calculate the temperature dependence of the average potential energy of the equilibrium liquid and show that it obeys the Rosenfeld–Tarazona $T^{3/5}$ law for low temperature T , while the average inherent structure energy is found to be inversely proportional to temperature at low T , consistent with a Gaussian distribution of potential energy minima. We investigate the shape of the basins around the local minima in configuration space via the average basin vibrational frequency and show that the basins become slightly broader upon cooling. We evaluate the configurational entropy S_{conf} , a measure of the multiplicity of potential energy minima sampled by the system, and test the validity of the AG relation between S_{conf} and the bulk dynamics. We quantify the dynamically heterogeneous motion by analyzing the motion of particles that are mobile on short and intermediate time scales relative to the characteristic bulk relaxation time. These mobile particles move in one-dimensional “strings”, and these strings form clusters with a well-defined average cluster size. The AG approach predicts that the *minimum* size of cooperatively rearranging regions (CRR) of molecules is inversely proportional to S_{conf} , and recently (Phys. Rev. Lett. **2003**, *90*, 085506) it has been shown that the mobile-particle clusters are consistent with the CRR envisaged by Adam and Gibbs. We test the possibility that the mobile-particle strings, rather than clusters, may describe the CRR of the Adam–Gibbs approach. We find that the strings also follow a nearly inverse relation with S_{conf} . We further show that the logarithm of the time when the strings and clusters are maximum, which occurs in the late- β -relaxation regime of the intermediate scattering function, follows a linear relationship with $1/TS_{\text{conf}}$, in agreement with the AG prediction for the relationship between the configurational entropy and the characteristic time for the liquid to undergo a transition to a new configuration. Since strings are the basic elements of the clusters, we propose that strings are a more appropriate measure of the *minimum* size of a CRR that leads to configurational transitions. That the cluster size also has an inverse relationship with S_{conf} may be a consequence of the fact that the clusters are composed of strings.

I. Introduction

Much of the current understanding of the properties of glass-forming liquids can be traced to the seminal theoretical and computational works of Frank Stillinger and his collaborators.¹ Stillinger was one of the pioneers of the topographic viewpoint of liquid thermodynamics and dynamics, first developed by Goldstein.² In this approach, the dynamics of a N -body system can be described as the motion of a point on a multidimensional potential energy hypersurface, referred to as the potential energy landscape (PEL). For a N -body system, the PEL refers to the system's potential energy U plotted as a function of $3N$ particle coordinates.² This surface consists of a large number of local

minima of varying depths, surrounded by potential energy barriers. At sufficiently low temperatures, the system resides near these local minima and the motion of the system can be described by vibrations around the minima, with infrequent transitions from one minimum to another.^{3,4}

The qualitative description of the potential energy landscape was formalized by Stillinger and Weber¹ using the concept of the inherent structures (IS), defined as the configuration of the system at a local minimum of the potential energy hypersurface. Stillinger defined a basin of attraction as the set of points that map to the same local minimum upon minimization of the potential energy. On the basis of this operational definition, Stillinger and Weber proposed a mathematical formalism—referred to as the inherent structure formalism—to quantify the thermodynamic properties of the PEL, where the degeneracy of energy minima can be related to the entropy. Since then, this approach has become an essential tool for understanding the dynamic and thermodynamic properties of glass-forming liquids,^{4–10} proteins,¹¹ and disordered spin systems.¹²

The IS formalism facilitates the direct calculation of the configurational entropy S_{conf} by computer simulation through the enumeration of basins in the PEL that are accessible to the

* To whom correspondence should be addressed. E-mail: sglotzer@umich.edu.

[†] University of Michigan.

[‡] Wesleyan University.

[§] Affiliation: Chemical Physics Program, Institute for Physical Sciences and Technology, University of Maryland, College Park, MD. Current address: Department of Chemistry, University of Utah. E-mail: yeshig@hec.utah.edu.

^{||} E-mail: fstarr@wesleyan.edu.

[⊥] New address: Westfälische Wilhelms-Universität Münster, Institut für Physikalische Chemie, Corrensstr. 30, D-48149 Münster, Germany; e-mail: mivogel@uni-muenster.de.

system in equilibrium. Direct evaluation of S_{conf} enabled testing of the phenomenological Adam–Gibbs (AG) theory that postulates a connection between thermodynamics and transport properties through a relation between S_{conf} and viscosity η . This AG relation has been successful in rationalizing the slowing down of the transport properties of many glass-forming liquids approaching T_g . According to the theory, relaxation in supercooled liquids takes place through the activated motion of cooperatively rearranging regions (CRR), defined as the smallest region that can undergo a transition to a new configuration without a requisite simultaneous configurational change on and outside its boundary.¹³ The theory also postulates that the CRRs grow upon cooling, and thus, relaxation slows down because a concerted motion of larger and larger groups of particles is required. This idea has been further considered by a number of authors.¹⁴

The notion that liquids approaching the glass transition should relax in dynamically correlated regions that have enhanced or diminished mobility relative to the average has received much attention over the past decade.^{15–31} This type of dynamics is commonly referred to as spatially heterogeneous dynamics.^{32–36} Numerous computer simulations^{39–46} and experimental works⁴⁷ have clearly identified transient correlated regions of enhanced mobility. These regions form well-defined clusters, that can typically be decomposed further into groups of particles or molecules that follow each other in a stringlike fashion.^{41,43,45} Quantification of the size of these dynamically active regions clearly demonstrates that their size increases as a glass transition is approached. A recent theory of dynamic facilitation predicts that spatially heterogeneous dynamics is a necessary consequence of local dynamical facilitation and cooperative motion.³⁶

Despite the progress in quantifying the nature of spatially heterogeneous dynamics (SHD), a direct connection to the CRR that is central to the AG theory has been elusive, in part because the size of the CRR is not precisely defined from microscopic quantities. The AG approach does provide a prediction for the relationship between the size z of a CRR and the configurational entropy, which provides a means to explore a possible relationship between the characteristic features of SHD and CRR. Recent work on a water model suggested that identifying z as the average size of a cluster of mobile particles may satisfy the predicted AG relation.⁴²

Given that clusters are comprised of smaller groups of particles that move together in “strings”, it is also natural to ask whether the strings may be a possible, if not a better, candidate to represent the CRR envisaged by Adam and Gibbs. Hence, the primary focus of this work is to explore the connection between the dynamical clusters and strings that have been found in earlier works and the CRR of the AG theory. Our approach is as follows: We first evaluate the configurational entropy and dynamical heterogeneity of a one-component liquid described by the Dzugutov potential, a model for simple metallic liquids. The calculations of S_{conf} are used to test the validity of the AG relation between S_{conf} and the diffusion coefficient. We then investigate the extent to which mobile-particle strings or clusters may represent the CRR by comparing several different measures of the characteristic string and cluster size to the “minimum cooperatively rearranging region” of the AG theory.

The paper is organized as follows. In section 2, we present the mathematical formalism that describes the thermodynamics of the IS, which can also be found in refs 1, 7, 9, 48, and 49. We then briefly describe our model in section 3. In section 4, we discuss the IS properties of our system. Section 5

describes the evaluation of configurational entropy in detail. The validity of the AG theory and the connection of CRR with the dynamical clusters and strings of highly mobile particles are explored in sections 6 and 7. The conclusion is given in section 8.

II. Inherent Structure Thermodynamic Formalism

The central idea of the IS formalism is the notion that, at sufficiently low T , the dynamics of a liquid can be separated into vibrations within a single basin and infrequent transitions between basins. This partitioning is motivated by the fact that at T approaching T_g , the time scales of intrabasin vibrational motion and interbasin diffusion differ by several orders of magnitude. Direct numerical evidence for the separation of the dynamics of a liquid into vibrations around and transitions between IS was provided by Schröder et al.,⁴ where such separation becomes possible in the vicinity of the mode-coupling temperature T_{MCT} . Stillinger recognized the consequence of this partitioning is that the canonical partition function can be conveniently rewritten as a sum over all of the local potential energy minima and an integral around the surrounding basins of attraction.¹

The canonical partition function of a system of N interacting particles is given by⁵⁰

$$Q_N(V, T) = \frac{h^{3N}}{N!} \int \int \exp[-\beta \mathcal{H}_N(\mathbf{r}^N, \mathbf{p}^N)] d\mathbf{r}^N d\mathbf{p}^N \quad (1)$$

where $\mathcal{H}_N(\mathbf{r}^N, \mathbf{p}^N)$ is the Hamiltonian of the system that is expressed as

$$\mathcal{H}_N(\mathbf{r}^N, \mathbf{p}^N) = \frac{1}{2m} \sum_{i=1}^N |\mathbf{p}_i|^2 + U_N(\mathbf{r}^N) \quad (2)$$

Here \mathbf{r}^N and \mathbf{p}^N are shorthand representations for the positions $\{\mathbf{r}_i\}$ and momenta $\{\mathbf{p}_i\}$ of the N particles, and $U_N(\mathbf{r}^N)$ is the total potential energy of the system. For the above Hamiltonian, the integration over the momenta can be carried out explicitly, and $Q_N(V, T)$ can be reduced to

$$Q_N(V, T) = \frac{\Lambda^{-3N}}{N!} Z_N(V, T) \quad (3)$$

where $\Lambda = (2\pi\beta\hbar^2/m)^{1/2}$ is the de Broglie thermal wavelength, $\beta = 1/k_B T$, and

$$Z_N(V, T) = \int \exp[-\beta U_N(\mathbf{r}^N)] d\mathbf{r}^N \quad (4)$$

is the configurational integral. In the IS formalism, the partitioning of the configuration space into nonoverlapping basins allows the partition function expressed above to be rewritten as¹

$$Q_N(V, T) = \Lambda^{-3N} \sum_{\text{basins}} \exp(-\beta e_{\text{IS}}) \int_{R_{\text{basin}}} \exp[-\beta(U_N - e_{\text{IS}})] d\mathbf{r}^N \quad (5)$$

where R_{basin} is the set of points comprising a specific basin and e_{IS} is the potential energy of the inherent structure corresponding to the basin. This last equation shows that the contributions to the partition function $Q_N(V, T)$ can be separated into two parts: the IS energy of all the distinct basins and the thermal excitation within the basins. If we introduce $\Omega(e_{\text{IS}}) de_{\text{IS}}$ as the density of

states with IS energy between e_{IS} and $e_{\text{IS}} + de_{\text{IS}}$, then the above equation can be written as

$$Q_N(V, T) = \int de_{\text{IS}} \Omega(e_{\text{IS}}) \exp[-\beta e_{\text{IS}} - \beta f_{\text{basin}}(\beta, e_{\text{IS}})] \quad (6)$$

where

$$-\beta f_{\text{basin}}(\beta, e_{\text{IS}}) = \ln \left(\int_{R(e_{\text{IS}})} \exp[-\beta(U_N - e_{\text{IS}})] \frac{d\mathbf{r}^N}{\Lambda^{3N}} \right) \quad (7)$$

Here, $f_{\text{basin}}(\beta, e_{\text{IS}})$ is interpreted as the basin free energy with IS energy e_{IS} . Equation 6 is further simplified if we define the configurational entropy $S_{\text{conf}}(e_{\text{IS}})$ as

$$S_{\text{conf}}(e_{\text{IS}}) = k_B \ln \Omega(e_{\text{IS}}) \quad (8)$$

Then, eq 6 becomes

$$Q_N(V, T) = \int de_{\text{IS}} \exp[-\beta(e_{\text{IS}} + f_{\text{basin}}(\beta, e_{\text{IS}}) - TS_{\text{conf}}(e_{\text{IS}}))] \quad (9)$$

In the thermodynamic limit, the free energy A of the system can be obtained from this equation by employing a maximum integrand evaluation, which yields

$$A = \bar{e}_{\text{IS}} - TS_{\text{conf}}(\bar{e}_{\text{IS}}) + f_{\text{basin}}(\beta, \bar{e}_{\text{IS}}) \quad (10)$$

Here, \bar{e}_{IS} is the average IS energy for a given T value that maximizes the integrand and thereby minimizes A .

The expression for the free energy eq 10 can be interpreted as follows. The first two terms on the right-hand side of eq 10 account for the average energy of the PEL minima visited and the degeneracy of the average IS energy \bar{e}_{IS} , respectively. The vibrational and the kinetic contributions are captured in the last term. Equation 10 thus provides a formal expression for the separation of configurational and vibrational contributions. Only an appropriate model for $f_{\text{basin}}(\beta, \bar{e}_{\text{IS}})$ is needed to fully evaluate S_{conf} ; we shall see that the basin free energy is dominated by harmonic contributions, as seen in other model glass-forming liquids,^{5,6,49} with small corrections from anharmonicities that we can include in an ad hoc fashion.

III. Model and Simulation

The model system we study is a one-component liquid using the Dzugutov interaction potential. The explicit form of the Dzugutov pair potential is⁵¹

$$\begin{aligned} V &= V_1 + V_2 \\ V_1 &= A(r^{-m} - B) \exp\left(\frac{c}{r-a}\right), \quad r < a \\ V_1 &= 0, \quad r \geq a \\ V_2 &= B \exp\left(\frac{d}{r-b}\right), \quad r < b \\ V_2 &= 0, \quad r \geq b \end{aligned} \quad (11)$$

where the parameters are compiled in Table 1. This pair potential is characterized by the presence of two repulsive regions and one attractive region. The potential is designed to favor local icosahedral ordering^{51,52} and is considered a generic model of simple metallic liquids, which have icosahedral coordination of the first neighbor shell. Further information about the model is found in refs 43 and 51.

TABLE 1: Parameter Values for the Potential in Eq 11⁵¹

m	A	c	a	B	d	b
16	5.82	1.1	1.87	1.28	0.27	1.94

Our molecular dynamics simulations are performed for a system of 2197 particles in a temperature range of $T = 0.44$ – 1.0 . For all of the state points studied, the simulations are performed at isothermal conditions and at a constant density $\rho = 0.85$. Periodic boundary conditions are used in all three of the spatial directions. For each T value studied, the liquid is cooled and equilibrated in a stepwise manner starting from $T = 1.6$. All of the units are quoted in Lennard-Jones reduced units: length in units of σ , temperature T in units of ϵ/k_B , and time in units of $\sigma(m/\epsilon)^{1/2}$. The mass m and the distance σ are set to unity.

To evaluate the entropy, we need to connect the range of densities and temperatures studied with the ideal gas. Hence, two additional sets of simulations are conducted. First, the system is simulated for temperatures ranging from $T = 2.0$ to $T = 5.0$ at constant density of $\rho = 0.85$. Then, a second set of simulations at $T = 5.0$ is carried out in the density range of 0.85 – 0.001 .

The number of particles used in the present simulation is smaller than the $N = 17\,576$ used in ref 43. The calculation of the configurational entropy involves the diagonalization of a large Hessian matrix, to be described below. To accomplish this task in a reasonable amount of time, we have reduced the system size to $N = 2197$. Unfortunately, these smaller systems have a tendency to crystallize in simulations when supercooled for moderate times.^{53,54} To exclude crystallizing configurations from our analysis and to improve statistics, we simulate many independent samples at each T and then remove those simulations that show a tendency toward crystal nucleation before beginning our analysis. The configurations that are crystallizing are identified by carefully inspecting the thermodynamic as well as the dynamic properties of each independent simulation. We use the behavior of the large system ($N = 17\,576$) as a benchmark and discard those configurations that have significantly different behavior. As a result, apart from its size, the properties of the system studied are within statistical error of that of the large system. Over all, our analysis is carried out by averaging over 23 independent simulations for the lowest T value, while as many as 100 independent simulations are used for higher temperatures.

IV. Inherent Structure Energy and Pair Distribution Function

As a first step toward characterizing the thermodynamics of the PEL, we sample the local potential energy minima nearest the system equilibrium trajectory on the PEL. This is accomplished by carrying out a conjugate gradient minimization^{55,56} of the potential energy starting from equilibrium liquid configurations, which are obtained from the molecular dynamics simulations. This process is often referred to as “quenching”. The associated quench rate is infinite, since T is set to zero before energy minimization. For a given temperature of the starting equilibrium configurations, at least 115 equilibrium configurations are mapped onto the respective inherent structure configurations.

A basic property characterizing the minima on the landscape is the average potential energy \bar{e}_{IS} . The temperature dependence of \bar{e}_{IS} has been studied by several authors.^{6,10,48,49,57–60} Figure 1 shows the plot of \bar{e}_{IS} as a function of T . As in the previous

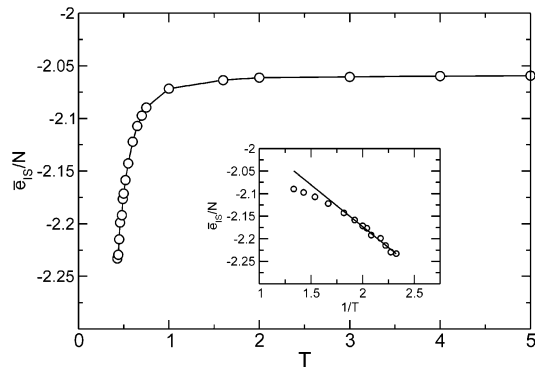


Figure 1. Average, inherent structure energy per particle \bar{e}_{IS}/N as a function of T . Inset: \bar{e}_{IS}/N (circle) as a function of the inverse temperature for $T \leq 0.75$. The solid straight line is a guide for the eye.

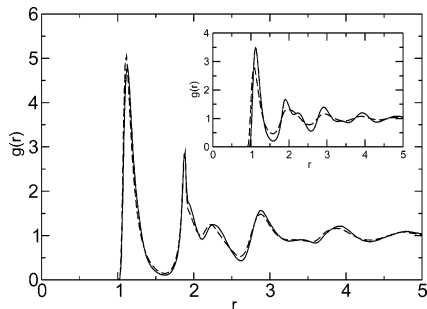


Figure 2. Inherent structure pair correlation function $g(r)$ for $T = 0.44$ (solid line) and $T = 1.0$ (dashed line). Inset: pair correlation function $g(r)$ for the equilibrium liquid for $T = 0.44$ (solid line) and $T = 1.0$ (dashed line).

studies, \bar{e}_{IS} is nearly constant at high T . The IS average energy decreases upon cooling below the “onset of caging”,⁶¹ indicating that the system populates deeper and deeper basins upon supercooling. Below this onset temperature, \bar{e}_{IS} is often found to follow a $1/T$ law for fragile liquids,^{10,48,49,57,58} which also appears true for this system (inset of Figure 1). This $1/T$ dependence has been mathematically shown to be a consequence of a Gaussian distribution of the probability density $P(e_{IS}, \beta)$.^{57,62,63}

To gain insight into the spatial distribution of particles in a given potential energy minimum, we measure the pair correlation function $g(r)$. The results for two different temperatures, $T = 0.44$ and $T = 1.0$, are shown in Figure 2. As first recognized by Stillinger and Weber,¹ the underlying structure obscured by the influence of vibrations in the equilibrium liquid becomes more apparent in the inherent structure. This is also the case for our system, where the splitting of the second peak in the pair correlation that arises from icosahedral ordering becomes sharper as compared to the equilibrium liquid.

V. Evaluation of Entropy

In this section, we present the methods and the results for the entropy S , as well as the configurational S_{conf} and vibrational S_{vib} contributions. The configurational entropy can be evaluated using two different methods, referred to as the histogram or PEL method and the thermodynamic integration (TI) method.⁷ The histogram method is based on constructing the probability distribution $P(e_{IS}, T)$ of the IS potential energy e_{IS} , which can be directly related to S_{conf} with one unknown constant.

In this study, we will employ the TI method, which uses the fact that, upon deep supercooling, the motion of particles in configurational space is separable into vibrations within a basin and infrequent transitions between basins. As a result, the total

entropy $S(T)$ can be expressed as the sum of the configurational entropy $S_{\text{conf}}(T)$ that results from the multiplicity of local potential energy minima sampled by the liquid and the vibrational entropy $S_{\text{vib}}(T)$ of typical basins sampled at T . Thus

$$S_{\text{conf}}(T) = S(T) - S_{\text{vib}}(T) \quad (12)$$

To obtain $S_{\text{conf}}(T)$, we need to evaluate both the overall $S(T)$, as well as the $S_{\text{vib}}(T)$. We will first focus on the evaluation of $S(T)$.

A. Total Entropy. To evaluate $S(T)$, we must connect our system with a reference system for which the exact value of S is known. In this case, we will use thermodynamic integration to connect our system with an ideal gas state.

Generally speaking, thermodynamic properties can be split into a contribution from the ideal gas, and a contribution from interactions, typically referred to as the “excess” over the ideal gas value. For example, the total entropy S can be written as $S = S^{\text{id}} + S^{\text{ex}}$, where S^{id} and S^{ex} are the ideal and excess terms of the entropy, respectively. Note that this should not be confused with the difference between the liquid and crystal entropies, sometimes also referred to as S^{ex} .

To determine the total entropy at a reference state point $R \equiv (T_R, V_R)$, where T_R and V_R are the reference temperature and volume, respectively, we perform thermodynamic integration at temperature $T_R = 5.0$ starting from a volume $V \rightarrow \infty$ (ideal gas limit) to the reference volume V_R (corresponding to density 0.85). Following ref 64, we need to evaluate

$$S(R) = S^{\text{id}}(R) + \frac{U(R)}{T} + \int_{\infty}^{V_R} \frac{P_{\text{ex}}}{T} dV \quad (13)$$

where $S^{\text{id}} = -\partial A^{\text{id}}/\partial T$ is expressed as⁶⁶

$$\frac{S^{\text{id}}}{k_B} = N \left[\ln \left(\frac{V}{N\Lambda^3} \right) + \frac{5}{2} \right] \quad (14)$$

To reduce the error in the numerical integration of P_{ex} in eq 13, we use the fact that $P_{\text{ex}} = B_2(T)k_B T(N/V)^2$ as $V \rightarrow \infty$, where $B_2(T)$ is the first nontrivial virial coefficient.⁶⁷ Therefore, we first subtract the virial term $B_2(T)T(N/V)^2$ from P_{ex} and then integrate the difference over the system volume. The contribution arising from the first virial correction is then integrated analytically and added to the remaining calculation. The resulting expression is

$$\int_{\infty}^{V_R} \frac{P_{\text{ex}}}{T} dV = \int_{\infty}^{V_R} \frac{1}{T} [P_{\text{ex}} - B_2(T)T \left(\frac{N}{V} \right)^2] dV - B_2(T) \frac{N^2}{V_R} \quad (15)$$

The values of the excess pressure $P_{\text{ex}} = P - P_{\text{id}}$ are plotted in Figure 3 as a function of V . From the behavior of P_{ex} at large V values, we find that $B_2(T) = 1.953$. Combining these elements, we find that the total entropy at the reference state point $S(R)/k_B = 18442$.

B. Entropy $S(T)$ at Different Temperatures. For a system with fixed N and V values, $dE = T dS$, where E is the total energy of the system. We can use this relationship to evaluate the entropy at any T along the isochoric path we study by integrating

$$S(T, V_R) = S(T_R, V_R) + \int_{T_R}^T \frac{dE}{T} \quad (16)$$

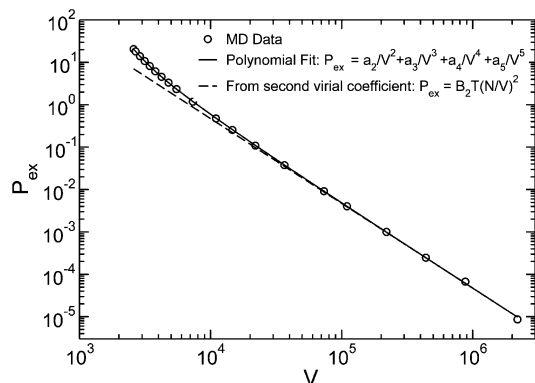


Figure 3. Excess pressure P_{ex} as a function of volume at $T = 5.0$. The open circles are the MD result. The dashed line is the fitting to the pressure using the first virial correction to the ideal gas law. The solid line is a polynomial fit.⁶⁵

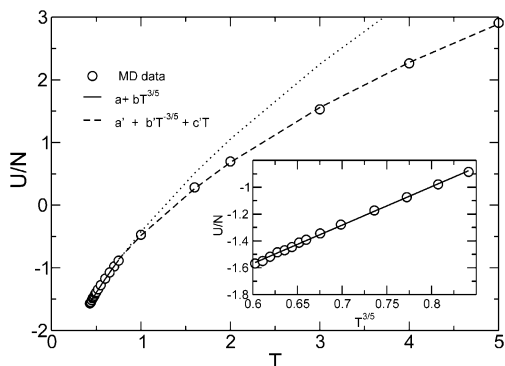


Figure 4. Potential energy per particle U/N (circles) of the equilibrium liquid plotted as a function of T . The temperature range $T \leq 0.75$ is fitted (solid line) using the functional form $U = a + bT^{3/5}$. The dashed line is a fitting to the data for the range $T \geq 0.75$ using the functional form $U = a' + b'T^{3/5} + c'T$. See refs 72 and 73 for the fit parameters. The dotted line, obtained from the fit of $U = a + bT^{3/5}$ for the entire T range, is shown to emphasize the extent of deviation of the potential energy from the Rosenfeld–Tarazona $T^{3/5}$ law for large T values, that is, $T \geq 1$. Inset: The data for $T \leq 0.75$ is separately plotted on $T^{3/5}$ axis to demonstrate that the Rosenfeld–Tarazona law⁶⁸ holds for low T .

The above equation may be rewritten in terms of the heat capacity C_V as

$$S(T, V_R) = S(T_R, V_R) + \int_{T_R}^T C_V(T) \frac{dT}{T} \quad (17)$$

where

$$C_V(T) = \frac{3}{2} Nk_B + \left(\frac{\partial U}{\partial T} \right)_V \quad (18)$$

To evaluate $\partial U/\partial T$ numerically, it is useful to have an analytic form for U that describes our exact numerical results from simulation. On the basis of the free energy functional calculation for hard spheres, Rosenfeld and Tarazona⁶⁸ showed that the temperature dependence of the potential energy of liquids can be described by $U(T) \sim T^{3/5}$. In a number of simulations,^{7,9,49,69,70} this theoretical prediction has been found to hold for sufficiently low T values. The potential energy for our system is also well represented by the form

$$U(T) = a + bT^{3/5} \quad (19)$$

for $T \leq 0.75$; see the inset of Figure 4.⁷² However, the Rosenfeld–Tarazona law does not hold for $T \geq 1.0$. For this

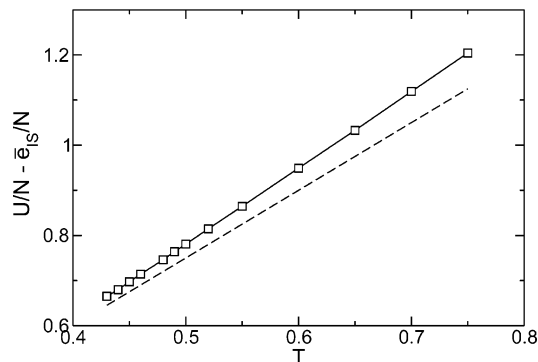


Figure 5. Harmonicity test. The difference between the average potential energy per particle U/N of the equilibrium liquid and the inherent structure \bar{e}_{is}/N is plotted as a function of T (open square). The dashed line is the harmonic approximation $U/N - \bar{e}_{\text{is}}/N = 3/2(1 - 1/N)k_B T$.

region, motivated by the functional form suggested in ref 49, we fit the simulation data using the form

$$U(T) = a' + b'T^{3/5} + c'T \quad (20)$$

As shown in Figure 4, this expression provides a good description of our numerical results for $T \geq 0.75$.⁷³ To determine $S(T)$ for $T \leq 0.75$, we first carry out an isochoric thermodynamic integration in the range of $T_R \geq T \geq 0.75$, using C_V obtained from the derivative of eq 20. This procedure links the entropy of the system $S(T_R)$ at the reference temperature $T_R = 5.0$ to that at 0.75. Then, we use C_V obtained from the derivative of eq 19 to calculate $S(T)$ at any $T < 0.75$. Figure 8 shows the plot of the total entropy $S(T)$ as a function of T obtained in this way.

C. Vibrational Entropy S_{vib} and Basin Shape. We next turn our attention to the vibrational component of S , which we will need to determine S_{conf} . Previous studies^{5–7,49} have shown that the vibration around the basin minima can be described predominately by a harmonic expansion around the minimum, with minor corrections due to higher order anharmonic terms. Thus, S_{vib} can be expressed as the sum of harmonic S_{harm} and the anharmonic S_{anh} terms.

To determine if it is necessary to include anharmonic corrections to S_{vib} , we first calculate the vibrational energy $U_{\text{vib}} = U/N - 3/2k_B T$; if the system is purely harmonic, $U_{\text{vib}} = 3/2k_B T$. Figure 5 shows that $U_{\text{vib}} > 3/2k_B T$, and thus there are higher order anharmonic terms that we must account for, as also found in the SPC/E model of water,⁵ the BKS model of silica,⁶ and the Lewis–Wahnström model of OTP.⁴⁹

1. Harmonic contribution to S_{vib} . We first focus our attention on the harmonic contribution to the vibrational entropy resulting from the motion of the system within the basins. This can be calculated using the relation

$$\frac{S_{\text{harm}}}{k_B} = \sum_{i=1}^{3N-3} \left[1 - \ln \left(\frac{\hbar \omega_i}{k_B T} \right) \right] \quad (21)$$

where $\{\omega_i\}$ values are the square roots of the eigenvalues of the Hessian matrix. The $3N \times 3N$ mass-weighted Hessian matrix elements H_{ij} are defined by

$$H_{ij} = \frac{1}{\sqrt{m_i m_j}} \frac{\partial^2 U}{\partial \mathbf{r}_i \partial \mathbf{r}_j} \Big|_{\mathbf{r}_{\alpha N}} \quad (22)$$

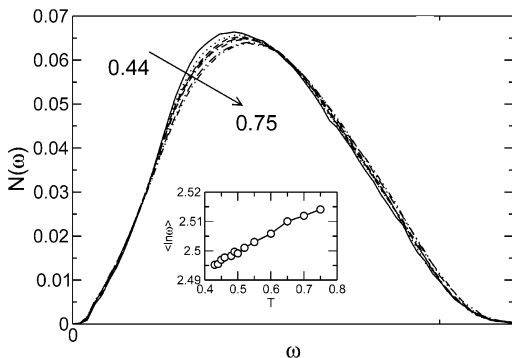


Figure 6. Density of states $N(\omega)$ at different temperatures. This quantity is the histogram of $\{\omega_i\}$. For clarity only selected temperature are shown. These are, along the direction of the arrow shown, $T = 0.44, 0.46, 0.49, 0.52, 0.55, 0.65,$ and 0.75 . Inset: $\langle \ln \omega \rangle$ as a function of T .

where m_i and m_j are the masses of particle i and j , respectively. These values are unity for our system. The Hessian matrix arises naturally by considering an expansion of U near a local minimum e_{IS} , that is,

$$U(\mathbf{r}^N) = e_{\text{IS}} + \sum_{i,j=1}^N (\mathbf{r}_i - \mathbf{r}_{\alpha i}) \frac{\partial^2 U}{\partial \mathbf{r}_i \partial \mathbf{r}_j} \Big|_{\mathbf{r}_{\alpha}} (\mathbf{r}_j - \mathbf{r}_{\alpha j}) + \text{higher order terms} \quad (23)$$

where \mathbf{r}_{α}^N is the $3N$ -dimensional IS configuration at the local minimum α . At the local minimum, the first derivative vanishes and $U(\mathbf{r}_{\alpha}^N) = e_{\text{IS}}$. Hence, the square roots of the eigenvalues, or normal modes $\{\omega_i\}$, provide a description of the curvature of the basin near the basin minimum. It is this curvature that we refer to as “basin shape”. Note that all of the $\omega_i \geq 0$ since they are evaluated at a local minimum; there are three zero eigenvalues that account for the three independent translational directions of the entire system.

To quantify the basin shape, we evaluate the density of states $N(\omega)$, which is the histogram of $\{\omega_i\}$ (Figure 6). The spectrum of $\{\omega_i\}$ changes weakly with T . Only the position of the maximum slightly shifts to smaller values of ω with decreasing T . To more closely inspect this change, we calculate the ensemble average of the sum of the logarithms of the frequencies of normal modes

$$\langle \ln \omega \rangle = \left\langle \frac{1}{3N-3} \sum_{i=1}^{3N-3} \ln \omega_i \right\rangle \quad (24)$$

This quantity captures the average quadratic shape of a basin. The T dependence of $\langle \ln \omega \rangle$ is shown in the inset of Figure 6. The $\langle \ln \omega \rangle$ value decreases weakly with decreasing T , indicating that basins become increasingly broad with increasing depth of the minima. Similar behavior has been found in the Lewis–Wahnström model of supercooled *o*-terphenyl (OTP).⁴⁹ The magnitude of the changes on cooling are small compared to water,⁴⁸ not unlike the binary LJ system.⁷¹ In contrast, in the SPC/E model of water⁴⁸ the average basin frequency increases upon cooling, and hence the basins in that system become increasingly “sharp” with decreasing basin energy.

Using the calculated values of ω_i at each T , we plot $S_{\text{harm}}(T)/k_B$ calculated using eq 21 in Figure 8.

2. Anharmonic Contribution to S_{vib} . To evaluate the anharmonic contribution to S_{vib} , we will exploit the fact that it is relatively easy to estimate the anharmonic contribution to

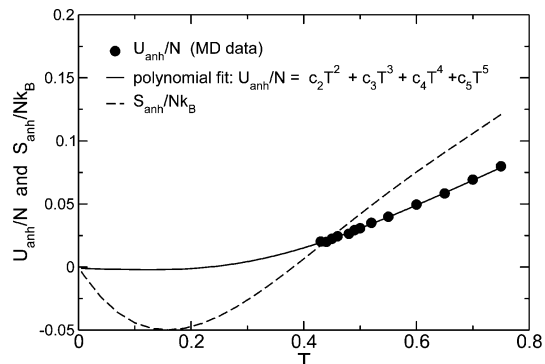


Figure 7. Anharmonic potential U_{anh} and entropy S_{anh} as a function of T . The filled circles represent the values of U_{anh} obtained from the simulation data through the relation given by eq 26. These data are fitted using eq 27 and extrapolated below the lowest T simulated, that is, below $T = 0.44$ (solid line). The dashed line represents S_{anh} that is evaluated using eq 25. This equation is further used to extend S_{anh} below $T = 0.44$ using a fit $S_{\text{harm}}/Nk_B = a_{\text{harm}} + b_{\text{harm}} \ln(T/T^*)$, where a_{harm} and b_{harm} are free fitting parameters found to be 2.86 and 2.896, respectively, and $T^* = 0.75$. The temperature dependence of S_{conf} is calculated as the difference between the total and the vibrational entropies.

the potential energy, U_{anh} , and then use the relation

$$S_{\text{anh}}(T) = \int_0^T \frac{1}{T'} \frac{\partial U_{\text{anh}}(T')}{\partial T'} dT' \quad (25)$$

where we have assumed that $S_{\text{anh}}(T=0) = 0$, as well as $S(T=0) = 0$, in accordance with the third law of thermodynamics for a liquid.

Recalling that eq 23 describes the expansion of U about a local minimum, the anharmonic contribution corresponds to the higher order terms in the expansion. Thus, U_{anh} can be approximated as

$$U_{\text{anh}}(T) = U(T) - \bar{e}_{\text{IS}}(T) - U_{\text{harm}}(T) \quad (26)$$

$U(T)$ and $\bar{e}_{\text{IS}}(T)$ are found from the simulation, while $U_{\text{harm}}(T) = \frac{3}{2}(N-1)k_B T$.

To perform the numerical integration of eq 25, the value of $U_{\text{anh}}(T)$ found from the simulation is further fitted to a polynomial in T to the order T^5 using the expression⁷⁴

$$U_{\text{anh}}(T) = \sum_{k=2}^5 c_k T^k \quad (27)$$

This form for U_{anh} requires that U_{anh} and its derivative with respect to T (the anharmonic contribution to specific heat) vanish at $T = 0$, as we would expect.

In Figure 7, we show the plot of U_{anh} and S_{anh} obtained from these calculations. Additionally, S_{anh} is plotted together with S and S_{harm} in Figure 8 to emphasize the extent of its contribution in the calculation of S_{conf} .

D. Configurational Entropy. Now that we have evaluated both $S(T)$ and $S_{\text{vib}}(T)$, we can evaluate $S_{\text{conf}} = S(T) - S_{\text{vib}}$. The plot of S_{conf} is shown in Figure 8 together with the plots of S , S_{harm} , and S_{anh} . Extrapolation of S_{conf} to lower T values using the fitting forms presented indicates that $S_{\text{conf}} \rightarrow 0$ at $T \approx 0.33$. In the PEL approach to liquid dynamics, when the number of accessible basins becomes intensive in the number of particles, the system can no longer explore phase space and is said to have reached a vitrified state of thermodynamic origin.⁷⁵ This state corresponds to $S_{\text{conf}} = 0$. The temperature where S_{conf} vanishes is frequently referred to as the Kauzmann temperature

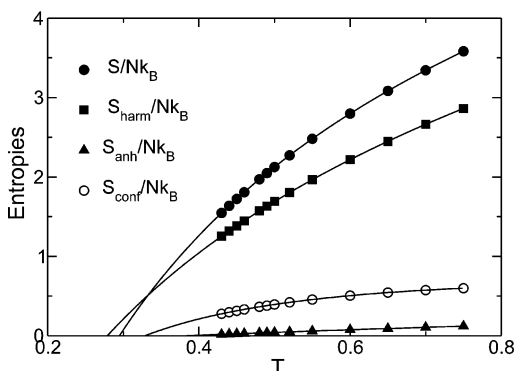


Figure 8. Total S , the harmonic S_{harm} , the anharmonic S_{anh} , and the configurational S_{conf} entropies as a function of T . S and S_{anh} are extended below $T = 0.44$, the lowest T simulated, using eq 17 and 25, respectively. On the other hand, S_{harm} is extended below $T = 0.44$ using a fit $S_{\text{harm}}/Nk_B = a_{\text{harm}} + b_{\text{harm}}(T/T^*)$, where a_{harm} and b_{harm} are free fitting parameters found to be 2.86 and 2.896, respectively, and $T^* = 0.75$. The temperature dependence of S_{conf} is calculated as the difference between the total and the vibrational entropies.

T_K . However, we should be careful to point out that the Kauzmann temperature originally refers to the temperature where the liquid and crystal entropies become equal. The relation between these definitions has been discussed elsewhere.^{75–77} Our estimate for T_K yields $T_K \approx 1.9 T_0$, where $T_0 = 0.1778$ is the so-called ideal glass-transition temperature obtained from the Vogel–Fulcher–Tammann fit. Apparently, our estimate for T_K is larger than the typical values documented in ref 79, where the measured values of T_K/T_0 are shown in the range $0.88 \leq T_K/T_0 \leq 1.39$. This disagreement could be a consequence of the fact that the extrapolation of the S_{conf} and D data are from higher T values (relative to T_{MCT}) than were used in other model liquids. We are restricted to these higher T values because of the tendency of the Dzugutov liquid to crystallize, as described in section III. Data at lower T values would reduce the amount of extrapolation in our fits and we expect would improve the agreement between T_0 and T_K . Nevertheless, the comparison of the estimated T_K value to the mode-coupling temperature $T_{\text{MCT}} \approx 0.443$,⁷⁸ estimated for the model yields the ratio $T_{\text{MCT}}/T_K \approx 1.21$. This ratio is within the range of observation for the SPC/E model of water for which a range of 1.20–1.35⁵ is estimated. The ratio T_{MCT}/T_K is one measure of the fragility of a liquid in which $T_{\text{MCT}}/T_K \rightarrow 1$ is expected for perfectly fragile liquids,⁸⁰ indicating that the Dzugutov liquid is fragile within the range of state points studied.

VI. Relation between S_{conf} and Bulk Dynamics

One of the main goals of this work is to explore the connection between the dynamic and thermodynamic properties of the Dzugutov supercooled liquid through the Adam–Gibbs (AG) relation. The AG theory¹³ has been tested for glass-forming liquids in the following form

$$D = D_0 \exp\left[\frac{-A}{TS_{\text{conf}}}\right] \quad (28)$$

This relation provides a connection between the dynamic and thermodynamic properties of the system. A wide range of systems have been found to obey this form of the Adam–Gibbs relation (see, e.g., refs 5, 7, and 49). To test the validity of this relation for our system we also plot $\log D$ against $1/TS_{\text{conf}}$ in Figure 9a. As illustrated in the figure, a linear relationship fits the data, but a careful inspection reveals that there is a slight, but systematic, curvature. A significant curvature has been

observed for the BKS model of silica⁶⁰ when $\log D$ is plotted against $1/TS_{\text{conf}}$, implying that the relation $D \propto \exp[-A/TS_{\text{conf}}]$, where A is a constant, may not be appropriate for silica. There, a better fit over a range of densities was obtained for the following relationship

$$D/T \propto \exp(-A/TS_{\text{conf}}) \quad (29)$$

Similarly, we find a better fit to a line when we plot $\log(D/T)$ against $1/TS_{\text{conf}}$ (Figure 9b). Note, however, the slight upward bend of the data at low T that remains. This behavior may indicate an enhanced value of the diffusion coefficient over that which would be predicted by the original Adam–Gibbs expression (see section VII.C) and the Stokes–Einstein relation^{30,32,81} and is not unexpected when substantial dynamical heterogeneity is present in the system,⁸² as is the case here.

VII. Dynamical Heterogeneity and Cooperatively Rearranging Regions

Central to the development of the AG approach is that motion of the system occurs through the independent relaxation of CRRs. The theory relates the minimum size of a cooperatively rearranging region z^* to the configurational entropy S_{conf} by

$$z^* \propto \frac{1}{S_{\text{conf}}} \quad (30)$$

However, as mentioned earlier, a precise microscopic definition of the CRR is lacking. Here we are particularly interested in assessing a possible connection between the CRR envisaged by the AG theory and the dynamic strings and clusters of mobile particles that are the signatures of spatially heterogeneous dynamics.

A. Mobile Particle Clusters and Strings. One way to quantify the nature of spatially heterogeneous motion is to identify clusters of mobile particles. These clusters are typically defined as sets of highly mobile particles that are within the first neighboring distance of each other.^{16,40} These clusters can also be separated into subsets of particles that replace each other along one-dimensional stringlike paths. These subsets are referred to as strings. Typically, the mobile particles that make up strings and clusters are identified by selecting the particles with the $\approx 5\%$ largest scalar displacement in a time interval t .^{15,16,39} Both clusters and strings have been reported in a number of different systems and were found to be relevant to the process of cage rearrangement, bulk relaxation, and exploration of the potential energy landscape.^{4,8,83}

We first focus on the mobile particle clusters. We identify two mobile particles as belonging to the same cluster if they are separated by a distance no greater than that of 1.5, the position of the first minimum of $g(r)$. By choosing many intervals t to define the mobility of particles, we can track the time evolution of these clusters. At any time, we can define a size of these clusters. There are two typical measures of the size: (i) the average size of a randomly chosen cluster, which we denote $S_n(t)$, and (ii) the average size of a cluster to which a randomly chosen molecule belongs, which we denote $S_w(t)$. The number-averaged cluster size is $S_n = \langle n \rangle$, where n is the number of particles in the cluster. The S_n value is dominated by smaller clusters and is a number average. The weight-averaged cluster size $S_w = \langle n^2 \rangle / \langle n \rangle$ gives more weight to larger clusters, since a randomly chosen particle is more likely in a large cluster.

A significant feature of the clusters is that, at any particular T , the mean size of the clusters is time dependent, with a peak

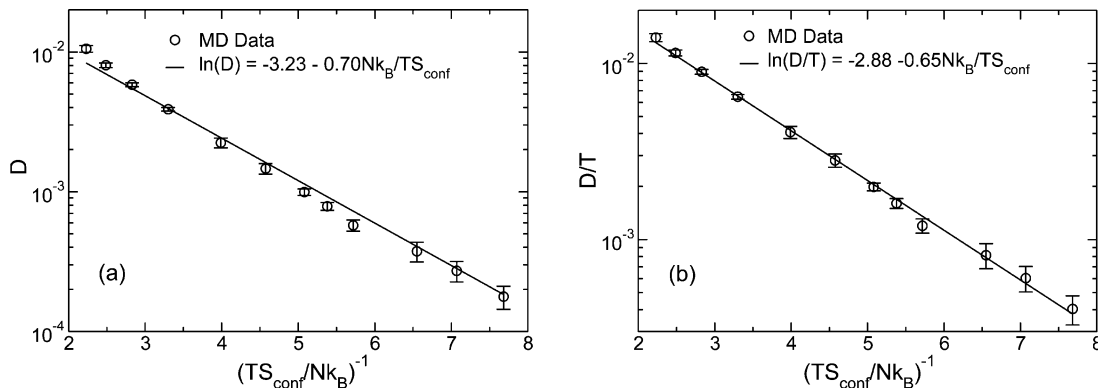


Figure 9. Test of the validity of the Adam–Gibbs theory for the Dzugutov liquid: (a) the diffusion coefficient D plotted against $1/TS_{\text{conf}}$ on a semilogarithmic axis and (b) D/T plotted against $1/TS_{\text{conf}}$ on a semilogarithmic axis.

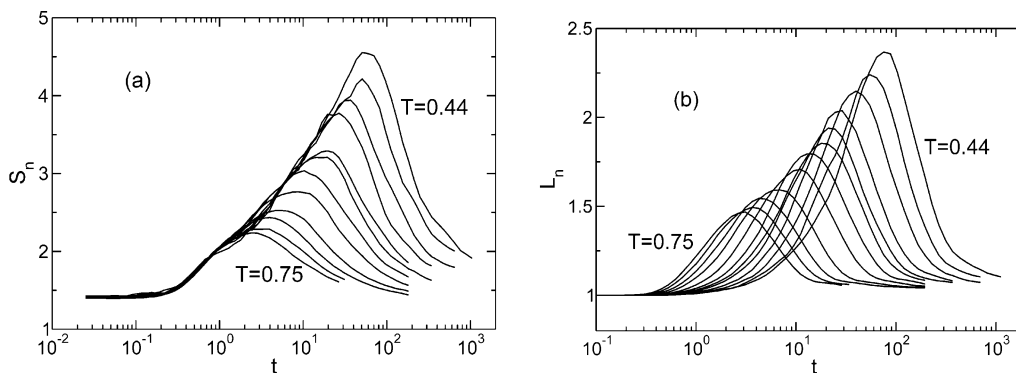


Figure 10. (a) Number averaged cluster size S_n and (b) the number averaged string size L_n plotted as a function of time. Note the strings are averaged over all of the strings including $l = 1$.

at intermediate time corresponding to the late- β -relaxation time of the MCT as shown in Figure 10a. For simplicity, we show only S_n , since the behavior of S_w is qualitatively nearly identical (the numerical values are larger for S_w). The maximum values of both S_n and S_w , which we denote S_n^* and S_w^* , increase with decreasing T , consistent with the phenomenological argument of the AG theory that requires z^* to increase as T decreases. Hence, the cluster size is one possible candidate to describe CRR, as we will discuss.

We next identify strings that aggregate to form larger, highly ramified clusters. Strings of mobile particles are identified by taking snapshots of configurations that are separated by a time interval t and then by finding highly mobile particles that replace each other within a radius $\delta = 0.6$ within the time interval t .^{15,43,45} Once the strings are found, we can define the mean size of the strings using either a number average L_n or a weight average L_w in analogy to the mobile particle clusters. Figure 10b shows that L_n has nearly the same qualitative behavior as S_n . Since strings are the components that make up the clusters and also match the qualitative expectations of the CRR of the AG approach, these are also viable candidates for the CRR. It is important to note that strings are not simply small clusters. Strings are identified by verifying both neighborhood and the direction of the displacements of particles, while neighborhood is the only criterion for clusters. Such directional correlations may owe its origin to the local structure, where dynamic facilitation is channeled through the local excitations.³⁶

B. Potential Candidates for Describing CRR. To explore the possible candidates for the CRR of the AG theory, and possibly identify the best measure of the CRR, we examine the linearity of the relationship between the number-averaged and weight-averaged mean values of the clusters and strings and

the inverse configurational entropy. In particular, we use the average values of the clusters and strings at the time when they are maximum to test the AG relation given in eq 30.

Strictly speaking, eq 30 requires that $z^* \rightarrow 0$ as $1/S_{\text{conf}} \rightarrow 0$. This requirement means that a linear fit between a measure, X , of the CRR and $1/S_{\text{conf}}$ must pass through the origin. With this in mind, we tested $X = S_n^*$, S_w^* , L_n^* , and L_w^* defined in the previous section. Of these four candidates, we find that only S_n^* and L_w^* obey a linear relationship with $1/S_{\text{conf}}$ that passes through the origin (Figure 11). A similar result for S_n^* was found in ref 42.; however, they found that $S_n^* - 1$ passes through the origin, and rationalized this by arguing that clusters of size one should not be considered CRR, and thus should be subtracted.

To better comprehend the variation in the intercept, we appeal to physical considerations that motivate a relaxation of the constraint that z^* should be zero only when $1/S_{\text{conf}}$ is zero. The AG relation was originally proposed for liquids near the glass transition; the limit of $1/S_{\text{conf}} \rightarrow 0$ refers to the infinite temperature limit. At high T , cooperativity is not important for particle motion, and so it is reasonable to expect that z^* should approach one at a finite value of T and thus before $1/S_{\text{conf}} \rightarrow 0$. As a result, the extrapolated value of z^* at the origin will be less than zero. Therefore, we relax the requirement that our fits should pass through the origin and test whether we obtain linear fits for $X - 1$ against $1/S_{\text{conf}}$, where we have subtracted one to eliminate those clusters or strings for which there is no cooperativity. We expect a fit of $X - 1$ vs $1/S_{\text{conf}}$ to pass through a positive, nonzero value of $1/S_{\text{conf}}$ at $X - 1 = 0$. We find a linear relationship for all of the candidates $X = S_n^*$, S_w^* , L_n^* , and L_w^* , as seen in Figures 12 and 13. Hence, all of these quantities are candidates for a measure of z^* .

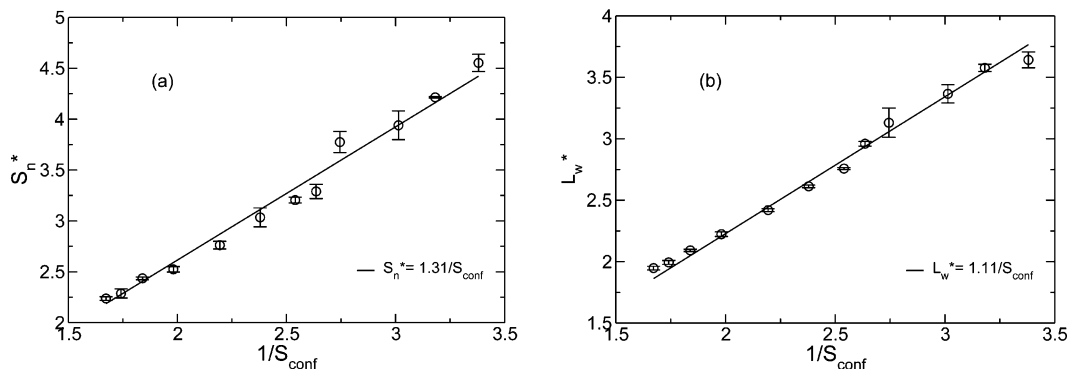


Figure 11. Plot of (a) S_n^* and (b) L_n^* against $1/S_{\text{conf}}$. These quantities are fitted using linear regression, where the fits are forced to pass through the origin.

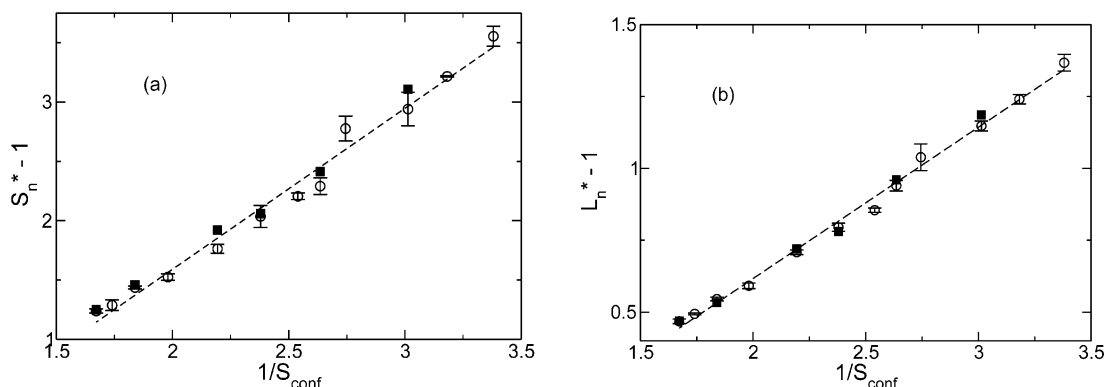


Figure 12. Plot of (a) $S_n^* - 1$ and (b) $L_n^* - 1$ against $1/S_{\text{conf}}$. S_n^* is the number-averaged mean cluster size S_n at the time $t_{\text{clu}}^{\text{max}}$ when S_n is maximum. L_n^* is the number-averaged mean string length L_n at the time $t_{\text{str}}^{\text{max}}$ when L_n is maximum. Open circles are data obtained from the small ($N = 2197$) system, and filled squares are data obtained from a big ($N = 17576$) system studied in ref 43.

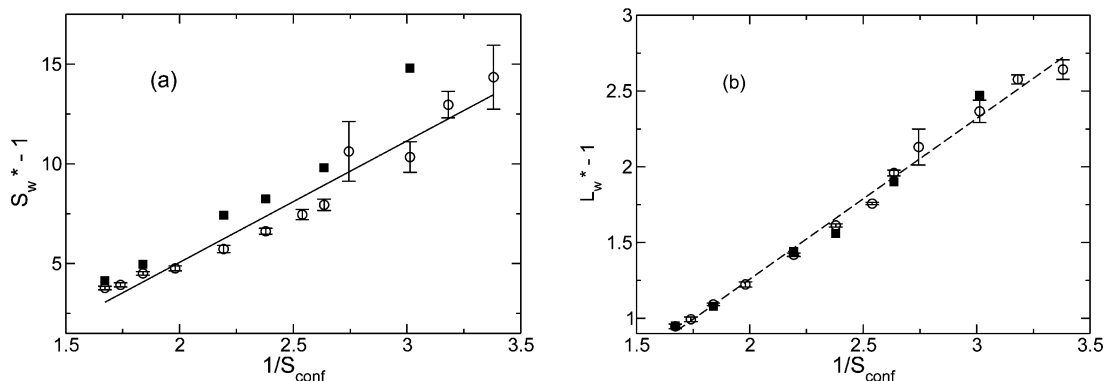


Figure 13. Plot of (a) $S_w^* - 1$ and (b) $L_w^* - 1$ against $1/S_{\text{conf}}$. S_w^* is the weight-averaged mean cluster size S_w at the time $t_{\text{clu}}^{\text{max}}$ when S_w is maximum. L_w^* is the weight-averaged mean string length L_w at the time $t_{\text{str}}^{\text{max}}$ when L_w is maximum. Open circles are data obtained from the small ($N = 2197$) system, and filled squares are data obtained from a big ($N = 17576$) system studied in ref 43.

At first glance, the plethora of possible measures for z^* is confusing. Which measure is most appropriate? To answer this question, we return to the formulation of the AG theory, where z^* in eq 30 refers to the *minimum* size that can give rise to a cooperative rearrangement. This naturally leads us to focus on the definition of z^* that is smallest and obeys eq 30. Therefore, we suggest that the string size is the more appropriate measure of the CRR. Why then should the cluster size follow eq 30, as found here and in ref 42? This is likely a result of the fact that the clusters consist of a collection of strings, which themselves obey the AG relation. But it is the strings, and not the clusters, that are the minimal units. Additionally, quantitative tests of the quality of the linear fit indicate that the linear fits to the string size are marginally better than those for the cluster size.

Figures 12 and 13 also include the weight-averaged and number-averaged mean cluster sizes and string sizes reported in ref 43 for a system containing 17 576 particles. Although we are unable to calculate S_{conf} in the large system, all of the other calculated bulk thermodynamic and dynamic quantities are indistinguishable within statistical error in the two systems, and thus we assume identical values for S_{conf} . The figures show that the weight-averaged cluster sizes (which are larger than the number-averaged cluster sizes) are diminished in the small system at low T , but the string sizes are essentially unchanged. This is expected since the largest clusters in the system exceed the smaller box size at low T , but the largest strings do not exceed the box size.⁴³ Thus, there are finite size effects in our measure of S_w^* , and so it is not reliable to compare it with the AG expression. All of the other quantities should be unaffected.

It would be valuable to revisit the water system where the cluster size was found to describe the CRR,⁴² to test if strings provide a better candidate for CRR in that system, as well as extending this analysis to other systems. As a final remark, we point out that a test of the AG relation that employs “micro-strings”, groups of particles that move coherently (that is, simultaneously) within strings (ref 43), may constitute an alternative candidate for the CRR, but that lies outside the scope of this work.

C. Characteristic Time of the AG Theory and Relation-ship to Configurational Entropy. In Adam and Gibbs' original paper,¹³ they proposed that the characteristic time required for the liquid to undergo a transition to a new configuration is proportional to the characteristic relaxation time of a cooperatively rearranging region. On this basis, they argued that

$$\tau_{\text{transition}} \propto \exp\left[\frac{A}{TS_{\text{conf}}}\right] \quad (55)$$

Since we have shown the strings (and clusters of strings) of highly mobile particles to be likely candidates for the CRRs, it is reasonable to propose that this characteristic time is given by the characteristic time of a string or cluster (which are essentially the same). We thus propose the following

$$t_{\text{str}}^{\text{max}} \propto \exp\left[\frac{A}{TS_{\text{conf}}}\right] \quad (56)$$

This expression is tested in Figure 14, where we see that a good linear fit is obtained when $\ln t_{\text{str}}^{\text{max}}$ is plotted vs $1/TS_{\text{conf}}$ over the admittedly limited number of decades available to us. The data for $t_{\text{clu}}^{\text{max}}$ is included in the figure for comparison. Unfortunately, the crystallization tendencies of the Dzugutov potential prevent us from obtaining equilibrium data at lower T values. It would be useful to test this expression in other liquids where additional decades in characteristic time scales are more easily obtainable. We note that a plot of either Dt^{max} or $(D/T)t^{\text{max}}$ vs T , for t^{max} corresponding to the time when the weight- or number-averaged string or cluster size is maximum, is not constant for all T values, demonstrating that the constant A in the numerator of the exponential of the AG expressions in eq 28 (or eq 29) and 31 is different in the two expressions. This is consistent with the derivation of the two expressions, which require several assumptions pertinent to the particular quantity under consideration.

VIII. Conclusion

One of the overarching goals of studying the correlated dynamics in supercooled liquids is to incorporate information about dynamic heterogeneities into theoretical approaches to the glass transition. To make progress in this direction, we need to identify connections between bulk relaxation phenomena and the strings and clusters of mobile particles. The approach presented by Adam and Gibbs proposes relations for the entropy with the bulk dynamics and the size of clusters. Combining these relations gives a possible direct theoretical connection between heterogeneity and relaxation.

By relating the average size S_n^* of mobile clusters to the diffusion constant D and the configurational entropy S_{conf} , Giovambattista et al. argued that S_n^* can be interpreted as the size of the CRR of the AG theory. Noting that the description of the CRR in the AG theory emerges from a heuristic argument, this connection sheds light into the possible origins of the AG theory, which has proved to be extremely useful over the last

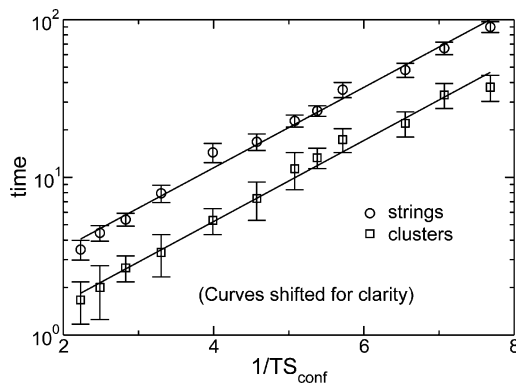


Figure 14. Plot of $\ln t_{\text{str}}^{\text{max}}$ and $\ln t_{\text{clu}}^{\text{max}}$ against $1/TS_{\text{conf}}$. $t_{\text{clu}}^{\text{max}}$ is the time when the weight-averaged mean cluster size S_w is maximum, and $t_{\text{str}}^{\text{max}}$ is the time when the weight-averaged mean string length L_w is maximum.

several decades to explain the nature of slowing dynamics in glass-forming liquids. Part of the motivation of this work was to explore the findings for mobile-molecule clusters in ref 42 for a different class of material; in so doing, we also investigated several predictions of the inherent structure formalism for the Dzugutov liquid. An additional motivation for this work was to explore to what extent strings, which include directional correlations not used to define mobile-particle clusters, may provide a better measure of the CRR of the AG theory.

We find that the temperature dependence of the average potential energy of the equilibrium liquid obeys the Rosenfeld–Tarazona $T^{3/5}$ law for low temperatures. Furthermore, the temperature dependence of the average inherent structure energy \bar{e}_{IS} is found to follow a $1/T$ law in the deeply supercooled regime, while \bar{e}_{IS} is essentially constant at high T . The shape of the basins around the local minima in configuration space, as detected by the average basin vibrational frequency, is observed to become slightly broader upon cooling similar to observations in the Lewis–Wahnström model of supercooled *o*-terphenyl (OTP) and in contrast to that observed for the SPC/E model of water in which the basins become increasingly sharp upon cooling.

We evaluated the configurational entropy S_{conf} of the Dzugutov liquid, and we investigated the validity of the Adam–Gibbs theory in that system. We find that the Adam–Gibbs relation between bulk dynamics and S_{conf} holds for the Dzugutov liquid at the studied T , as was observed in other systems. We also explored the connection between the dynamical clusters or strings that are the signatures of spatially heterogeneous dynamics, and the CRRs of the Adam–Gibbs theory. Similar to the observation for the SPC/E model of water, we find a linear relationship between the size of mobile-particle clusters and $1/S_{\text{conf}}$, which in turn provides a possible connection between clusters and the CRR. We further tested the possible relationship between the size of mobile-particle strings and S_{conf} and found a marginally better linear relationship than that found for the cluster size. This marginal difference between the strings and the clusters in better describing the CRR is likely a consequence of the fact that clusters are themselves composed of strings. Nonetheless, the fact that strings show a slightly better linear relationship, combined with the fact that these are the more elementary units of cooperativity, suggests that strings are better candidates for the CRR within the language proposed by the AG theory. We performed tests of the characteristic time of the string and cluster size as the characteristic relaxation time of the AG theory, which further support this proposition. Simulations that are able to probe T values will be

valuable, as the range over which we have been able to test this relation is relatively limited because of the crystallization tendencies of the Dzugutov liquid at lower T values.

Acknowledgment. We are grateful to the University of Michigan Center for Advanced Computing for support of our computer cluster. We thank S. Sastry and T. Schröder for providing us with the energy minimization code, sections of which were used for portions of this study. S.C.G. thanks Frank Stillinger for many enlightening discussions on the nature of the glass transition. M.V. gratefully acknowledges funding of Deutsche Forschungsgemeinschaft through the Emmy Noether-Programm.

References and Notes

- Stillinger, F. H.; Weber, T. A. *Phys. Rev. A* **1982**, *25*, 978; *Phys. Rev. A* **1983**, *28*, 2408; *J. Phys. Chem.* **1983**, *87*, 2833; *Science* **1984**, *225*, 983; *J. Chem. Phys.* **1984**, *80*, 4434; *J. Chem. Phys.* **1985**, *83*, 4767; *Science* **1995**, *267*, 1935.
- Goldstein, M. J. *J. Chem. Phys.* **1969**, *51*, 3728.
- Büchner, S.; Heuer, A. *Phys. Rev. E* **1999**, *60*, 6507. Büchner, S.; Heuer, A. *Phys. Rev. Lett.* **2000**, *84*, 2168. Doliwa, B.; Heuer, A. *Phys. Rev. E* **2003**, *67*, 030501.
- Schröder, T. B.; Sastry, S.; Dyre, J. C.; Glotzer, S. C. *J. Chem. Phys.* **2000**, *112*, 9834.
- Scala, A.; Starr, F. W.; La Nave, E.; Sciortino, F.; Stanley, H. E. *Nature* **2000**, *406*, 166.
- Voivod, I. S.; Poole, P. H.; Scortino, F. *Nature* **2001**, *412*, 514.
- Sastry, S. *Phys. Rev. Lett.* **2000**, *85*, 590; *Nature* **2001**, *409*, 164; *J. Phys.: Condens. Matter* **2000**, *12*, 6515.
- Vogel, M.; Doliwa, B.; Heuer, A.; Glotzer, S. C. *J. Chem. Phys.* **2004**, *120*, 4404.
- Sciortino, F.; Kob, W.; Tartaglia, P. *Phys. Rev. Lett.* **1999**, *83*, 6331.
- Sastry, S.; Debenedetti, P. G.; Stillinger, F. H. *Nature* **1998**, *393*, 554.
- Frauenfelder, H.; Sligar, S. G.; Wolynes, P. G. *Science* **1991**, *254*, 1598. Abkevich, V. I.; Gutin, A. M.; Shakhnovich, E. I. *J. Chem. Phys.* **1994**, *101*, 6052. Saven, J. G.; Wang, J.; Wolynes, P. G. *J. Chem. Phys.* **1994**, *101*, 11037. Wang, J.; Onuchic, J.; Wolynes, P. G. *Phys. Rev. Lett.* **1996**, *76*, 4861. Dill, K. A.; Chan, H. S. *Nat. Struct. Biol.* **1997**, *4*, 10. Nienhaus, G. U.; Müller, J. D.; McMahon, B. H.; Frauenfelder, H. *Physica D* **1997**, *107*, 297.
- Stillinger, F. H. *Physica D* **1987**, *107*, 383. Beaton, D. A.; DeCoste, C.; Hunter, D. L.; Coniglio, A. *Int. J. Mod. Phys. C* **2000**, *11*, 41. Crisanti, A.; Ritort, F. *Europhys. Lett.* **2000**, *52*, 640.
- Adam, G.; Gibbs, J. H. *J. Chem. Phys.* **1965**, *43*, 139.
- Donth, E. J. *J. Non-Cryst. Solids* **1991**, *131*, 204. Moynihan, C. T.; Schroeder, J. *J. Non-Cryst. Solids* **1993**, *160*, 52. Sappelt, D.; Jäckle, J. *J. Phys. A* **1993**, *26*, 7325. Mohanty, U. *Adv. Chem. Phys.* **1995**, *89*, 89. *J. Chem. Phys.* **1994**, *100*, 5905. Ediger, M. D. *J. Non-Cryst. Solids* **1998**, *235*, 10.
- Donati, C.; Douglas, J. F.; Kob, W.; Poole, P. H.; Plimpton, S. J.; Glotzer, S. C. *Phys. Rev. Lett.* **1998**, *80*, 2338.
- Donati, C.; Glotzer, S.; Poole, P.; Kob, W.; Plimpton, S. *Phys. Rev. E* **1999**, *60*, 3107.
- Glotzer, S. C.; Donati, C. *J. Phys.: Condens. Matter* **1999**, *11*, A285. Donati, C.; Glotzer, S. C.; Poole, P. H. *Phys. Rev. Lett.* **1999**, *82*, 5064. Bennemann, C.; Donati, C.; Baschnagel, J.; Glotzer, S. C. *Nature* **1999**, *399*, 246. Poole, P. H.; Donati, C.; Glotzer, S. C. *Physica A* **1998**, *261*, 51. Glotzer, S. C.; Donati, C.; Poole, P. H. *Computer Simulation Studies in Condensed Matter Physics XI*, Landau, D. P., Ed.; Springer-Verlag: New York, 1999. Allegrini, P.; Douglas, J. F.; Glotzer, S. C. *Phys. Rev. E* **1999**, *60*, 5714.
- Heuer, A.; Okun, K. *J. Chem. Phys.* **1997**, *106*, 6176. Doliwa, B.; Heuer, A. *Phys. Rev. Lett.* **1998**, *80*, 4915. Heuer, A.; Wilhelm, M.; Zimmerman, H.; Spiess, H. W. **1995**, *75*, 2851. Tracht, U.; Wilhelm, M.; Heuer, A.; Feng, H.; Schmidt-Rohr, K.; Spiess, H. W. *Phys. Rev. Lett.* **1998**, *81*, 2727.
- Hiwatari, Y.; Muranaka, T. *J. Non-Cryst. Solids* **1998**, *235*, 19.
- Perera, D. N.; Harrowell, P. *J. Non-Cryst. Solids* **1998**, *235*, 314. Perera, D. N.; Harrowell, P. *J. Chem. Phys.* **1999**, *111*, 5441.
- Yamamoto, R.; Onuki, A. *Phys. Rev. E* **1998**, *58*, 3515.
- Johnson, G.; Mel'cuk, A.; Gould, H.; Klein, W.; Mountain, R. D. *Phys. Rev. E* **1998**, *57*, 5707.
- Schmidt-Rohr, K.; Spiess, H. W. *Phys. Rev. Lett.* **1991**, *66*, 3020.
- Chang, I.; Fujara, F.; Geil, B.; Heuberger, G.; Mangel, T.; Sillescu, H. *J. Non-Cryst. Solids* **1994**, *172–174*, 248. Heuberger, G.; Sillescu, H. *J. Phys. Chem.* **1996**, *100*, 15255.
- Marcus, A. H.; Schofield, J.; Rice, S. A. *Phys. Rev. E* **1999**, *60*, 5725.
- Cicerone, M. T.; Ediger, M. D. *J. Chem. Phys.* **1995**, *103*, 5684.
- Schiener, B.; Chamberlin, R. V.; Diezemann, G.; Bohmer, R. *J. Chem. Phys.* **1997**, *107*, 7746.
- Hinze, G. *Phys. Rev. E* **1998**, *57*, 2010.
- Leisen, J.; Schmidt-Rohr, K.; Spiess, H. W. *Physica A* **1993**, *201*, 3020. Böhmer, R.; Hinze, G.; Diezemann, G.; Geil, B.; Sillescu, H. *Europhys. Lett.* **1996**, *36*, 55. Kuebler, S. C.; Heuer, A.; Spiess, H. W. *Phys. Rev. E* **1997**, *56*, 741. Böhmer, R.; Diezemann, G.; Hinze, G.; Sillescu, H. *J. Chem. Phys.* **1998**, *108*, 890.
- Ediger, M. D. *Annu. Rev. Phys. Chem.* **2000**, *51*, 99.
- Kegel, W. K.; Blaaderen, A. V. *Science* **2000**, *287*, 290.
- Stillinger, F. H.; Hodgdon, J. A. *Phys. Rev. E* **1994**, *50*, 2064.
- Böhmer, R. *Curr. Opin. Solid State Mater. Sci.* **1998**, *3*, 378; Böhmer, R.; et al. *J. Non-Cryst. Solids* **1998**, *235*, 1.
- Sillescu, H. *J. Non-Cryst. Solids* **1999**, *243*, 81.
- Glotzer, S. C. *J. Non-Cryst. Solids* **2000**, *274*, 342.
- Garrahan, J. P.; Chandler, D. *Phys. Rev. Lett.* **2002**, *89*, 035704. Garrahan, J. P.; Chandler, D. *Proc. Natl. Acad. Sci. U.S.A.* **2003**, *100*.
- Robertson, R. E. *J. Polym. Sci., Polym. Symp.* **1978**, *63*, 173. Donth, E. J. *J. Non-Cryst. Solids* **1982**, *53*, 325; **1991**, *131*, 204. *Relaxation and Thermodynamics in Polymers: Glass Transition*; Akademie Verlag: Berlin, Germany, 1992. Moynihan, C. T.; Schroeder, J. *J. Non-Cryst. Solids* **1993**, *160*, 52; **1993**, *161*, 148. Mohanty, U. *Adv. Chem. Phys.* **1995**, *89*, 89; Ediger, M. D. *J. Non-Cryst. Solids* **1998**, *235*, 10.
- Sappelt, D.; Jäckle, J. *J. Phys. A: Math. Gen.* **1993**, *26*, 7325. Donati, C.; Jäckle, J. *J. Phys.: Condens. Matter* **1996**, *8*, 2733.
- Kob, W.; Donati, C.; Plimpton, S. J.; Poole, P. H.; Glotzer, S. C. *Phys. Rev. Lett.* **1997**, *79*, 2827.
- Gebremichael, Y.; Schröder, T. B.; Starr, F. W.; Glotzer, S. C. *Phys. Rev. E* **2001**, *64*, 051503.
- Gebremichael, Y.; Vogel, M.; Glotzer, S. C. *Mol. Simul.* **2004**, *30*, 281.
- Giovambattista, N.; Buldyrev, S. V.; Starr, F. W.; Stanley, H. E. *Phys. Rev. Lett.* **2003**, *90*, 085506; *Phys. Rev. E*, *72*, in press.
- Gebremichael, Y.; Vogel, M.; Glotzer, S. C. *J. Chem. Phys.* **2004**, *120*, 4415.
- Vogel, M.; Glotzer, S. C. *Phys. Rev. Lett.* **2004**, *92*, 255901.
- Aichele, M.; Gebremichael, Y.; Starr, F. W.; Baschnagel, J.; Glotzer, S. C. *J. Chem. Phys.* **2003**, *119*, 5290.
- Lacevic, N.; Starr, F. W.; Schröder, T. B.; Novikov, V. N.; Glotzer, S. C. *Phys. Rev. E* **2002**, *66*, 030101(R).
- Weeks, E.; Crocker, J. C.; Levitt, A. C.; Schofield, A.; Weitz, D. A. *Science* **2000**, *287*, 627.
- Starr, F. W.; Sastry, S.; La Nave, E.; Scala, A.; Stanley, H. E.; Sciortino, F. *Phys. Rev. E* **2001**, *63*, 041201.
- Mossa, S.; La Nave, E.; Stanley, H. E.; Donati, C.; Sciortino, F.; Tartaglia, P. *Phys. Rev. E* **2002**, *65*, 041205.
- Hansen, J. P.; McDonald, I. R. *Theory of Simple Liquids*; Academic Press: London, 1986.
- Dzugutov, M.; Larsson, K.-E.; Ebbsjö. *Phys. Rev. A* **1988**, *38*, 3609. Dzugutov, M. *Phys. Rev. A* **1992**, *46*, R2984. Dzugutov, M. *J. Non-Cryst. Solids* **1993**, *156*, 173. Zetterling, F.; Dzugutov, M.; Simdyankin, S. *J. Non-Cryst. Solids* **2001**, *293*, 39.
- Doye, J. P. K.; Wales, D. J.; Zetterling, F. H. M.; Dzugutov, M. *J. Chem. Phys.* **2003**, *118*, 2792.
- Debenedetti, P. G. *Metastable Liquids: Concepts and Principle*; Princeton University Press: Princeton, NJ, 1996.
- Shell, M. S.; Debenedetti, P. G.; Stillinger, F. H. *J. Phys. Chem. B* **2004**, *108*, 6772.
- Press, W. H.; Teukolsky, S. A.; Vetterling, W. T.; Flannery, B. P. *Numerical Recipes in C, The Art of Scientific Computing*, 2nd ed.; Cambridge University Press: New York, 1988.
- The conjugate gradient code we used for minimization was originally developed by S. Sastry and T. Schröder and later modified by M. Bergroth.
- Heuer, A. *Phys. Rev. Lett.* **1997**, *78*, 4051. Buechner, S.; Heuer, A. *Phys. Rev. E* **1999**, *60*, 6507.
- La Nave, E.; Sciortino, F.; Tartaglia, P.; De Michele, C.; Mossa, S. *J. Phys.: Condens. Matter* **2003**, *15*, S1085.
- Sastry, S. *Physica A* **2002**, *315*, 267.
- Voivod, I. S.; Sciortino, F.; Poole, P. H. cond-mat/0309481.
- The onset of caging for this system is identified from the emergence of a plateau regime in the intermediate scattering function $F(q,t)$ or the mean square displacement $\langle r^2 \rangle$ measured in refs 41 and 43.
- Speedy, R. J. *J. Phys. Chem. B* **1999**, *103*, 4060.
- Speedy, R. J.; Debenedetti, P. G. *Mol. Phys.* **1998**, *88*, 1293.
- Sciortino, F.; Kob, W.; Tartaglia, P. Proceedings of Unifying Concepts in Glass Physics, Trieste, Italy, 1999; *J. Phys.: Condens. Matter* **2000**, *12*, 6525.

(65) The constants in the polynomial fit to P_{ex} are $a_2 = 4.71 \times 10^7$, $a_3 = 1.42 \times 10^{11}$, $a_4 = -3.37 \times 10^{14}$, and $a_5 = 1.47 \times 10^{18}$. The a_2 value is directly related to B_2 .

(66) To evaluate eq 14, we use $\hbar = 0.063507$ kJ ps mol⁻¹ and assume the unit of energy to be $\epsilon = 1$ kJ mol⁻¹, the unit of length to be $\sigma = 1$ nm, and the unit of time to be $\tau = 1$ ps. We obtain $S^{\text{id}}(R)/k_B = 23\,265.5$ using these values. Note that the choice of constants will play no role when we return to reduced units.

(67) Landau, L. D.; Lifshitz, E. M. *Statistical Physics*, 3rd ed; Pergamon Press: Oxford, U.K., 1980; part 1.

(68) Rosenfeld, Y.; Tarazona, P. *Mol. Phys.* **1998**, *95*, 141.

(69) Scala, A.; Starr, F. W.; La Nave, E.; Stanley, H. E.; Sciortino, F. *Phys. Rev. E* **2000**, *62*, 8016.

(70) Coluzzi, B.; Parisi, G.; Verrocchio, P. *J. Chem. Phys.* **2000**, *112*, 2933.

(71) Kob, W.; Sciortino, F.; Tartaglia, P. *Europhys. Lett.* **2000**, *49*, 590. Sciortino, F.; Tartaglia, P. *Phys. Rev. Lett.* **2001**, *86*, 107.

(72) The best fit of U using eq 19 yields $a = -7221.98$ and $b = 6292.87$, in the temperature range $T \leq 0.75$.

(73) The best fit of U using eq 20 yields $a' = -6771.84$, $b' = 6492.36$, and $c' = -785.32$. It is interesting to note that with a different set

of fitting parameters, this functional form can describe the entire T range of the simulation data.

(74) The coefficients c_k we find for eq 27 are $c_2 = -783.2$, $c_3 = 4500.3$, $c_4 = -6241.1$, and $c_5 = 2917.6$.

(75) Debenedetti, P. G.; Stillinger, F. H. *Nature* **2001**, *410*, 259.

(76) Stillinger, F. H.; Debenedetti, P. G.; Truskett, T. M. *J. Phys. Chem. B* **2001**, *105*, 11809.

(77) Starr, F. W.; Angell, C. A.; Stanley, H. E. *Physica A* **2003**, *323*, 51.

(78) Dzugutov, M.; Simdyankin, S. I.; Zetterling, F. H. M. *Phys. Rev. Lett.* **2002**, *89*, 195701-1.

(79) Angell, C. A. *Physica D* **1997**, *107*, 122.

(80) Angell, C. A. *Science* **1995**, *267*, 1924.

(81) Hall, D. D.; Deppe, D. D.; Hamilton, K. E.; Dhinojwala, A.; Torkelson, J. M. *J. Non-Cryst. Solids* **1998**, *235*, 48.

(82) Glotzer, S. C.; Novikov, V. N.; Schröder, T. B. *J. Chem. Phys.* **2004**, *112*, 509.

(83) Denny, R. A.; Reichman, D. R.; Bouchaud, J.-P. *Phys. Rev. Lett.* **2003**, *90*, 025503; Monthus, C.; Bouchaud, J.-P. *J. Phys. A* **1996**, *29*, 3847.